Pergamon

Int. J. Heat Mass Transfer. Vol. 38, No. 9, pp. 1637–1645, 1995

0017-9310/95 $9.50+0.00

0017-9310(94)00293-2

Melting and solidification of thin wires: a class of phase-change problems with a mobile interface—I. Analysis

L. J. HUANG

Harrison Radiator, Division of General Motors Corporation, Lockport, NY 14094-1896, U.S.A.

and

P. S. AYYASWAMY† and I. M. COHEN

Department of Mechanical Engineering and Applied Mechanics, University of Pennsylvania, Philadelphia, PA 19104-6315, U.S.A.

(*Received* 24 *March* 1994 *and in final form* 11 *August* 1994)

Abstract—In this paper, a model that describes the transient heating of a thin wire causing the tip to melt, roll-up of the molten mass into a ball due to surface tension forces, and the subsequent solidification of the molten material due to conduction up the wire and convection and radiation from the surface, has been provided. The wire is assumed to be heated at its lower tip to a temperature beyond the melting temperature of the wire material by heat flux from an electrical discharge. The shape of the melt is analytically/numerically determined by solving equations based on minimum energy principles. The departure from sphericity of the melt that is formed is examined by perturbation schemes, based on expansions for small ratio of gravity to surface tension forces and small ratio of surface tension gradient to surface tension forces, both of which are true for the problems considered. Temperature fields in the melt have been obtained by solving the energy equation using a body-fitted coordinate system. Temperature fields in the wire above the melt were calculated as well. Comparisons of those temperatures with experimental measurements described in Part II of this study are excellent.

1. INTRODUCTION

We examine the heating of a thin wire by heat flux supplied at one end. The heat supplied eventually causes the tip to melt. As the wire melts, surface tension forces cause the melt to roll-up and form a ball shaped object. When the heating is terminated, the melt cools and solidifies due to heat loss by conduction up the wire and convection and radiation from the surface. The analyses and numerical simulations described in this study examine all of the constituent aspects of such processes. We start with a long fine wire. The initial heat-up is governed by a nonlinear transient heat conduction equation. The nonlinearity arises from the presence of the radiative heat loss to the ambient. The melting problem involves a careful consideration of the mobile phase change interface. By a suitable coordinate transformation, we immobilize the interface and describe the problem in fixed coordinates. The shape of the liquid melt is derived by an extremum principle which guarantees a minimum total energy for a given volume of melt. The effects of temperature variation on surface tension and the effect of gravity are taken into account in deriving the shape of the melt. The variational procedure associated with the extremum principle results in the derivation of an Euler–Lagrange equation for the surface shape at each instant of time. The energy equation for the molten and solid regions are simultaneously solved by finite differences using body-fitted coordinates. The computational grid is allowed to change with time as the phase change interface is maintained coincident with a fixed mesh line. The interface conditions with phase change and the energy equations for the liquid and solid regions are developed in a general non-orthogonal coordinate system suitable for the numerical calculation. The timewise temperature distribution in the solid phase is obtained by a numerical calculation. The timewise temperature distribution in the solid phase is obtained by a Crank–Nicolson solution algorithm for the energy equation. Finally, comparisons for shape predictions and temperature fields are made between the numerical results and both experimental measurements and photographs developed using high speed films. In the experiments, described in Part II, fine aluminum and copper wires are subject to electric arc heating in a partially evacuated chamber or with a suitable cover gas (see Fig. 1). The corresponding current, pressure and temperature values are recorded.

† Author to whom correspondence should be addressed.

NOMENCLATURE

a_{11}, a_{12}, a_{22} coefficients defined by equation (56)
c_p specific heat [J kg^{-1} K^{-1}]
D bottom of the ball
Eo Eötvös number ($g\rho_l R_w^2/\sigma_m$)
f fraction
g acceleration due to gravity [m s^{-2}]
h heat transfer coefficient [W m^{-2} K^{-1}]
J coefficient defined by equation (56)
k thermal conductivity [W m^{-1} K^{-1}]
L length of the wire (scaled by R_w)
n_b, n_w outward drawn normal from the ball surface (b), melt interface (w)
p pressure
P, Q coordinate control functions
r radial coordinate (scaled by R_w)
R radius [m]
t time [s]
T temperature ($T-T_m$) [K]
V volume (scaled by πR_w^3)
x x-coordinate (scaled by R_w).

Greek symbols
α thermal diffusivity [m^2 s^{-1}]
β, γ fractions of the spacings used in finite differencing
Γ Lagrange multiplier
ε emissivity; $(\sigma-\sigma_m)/\sigma_m$
δ ε/θ_s, defined by equation (28)
η coordinate direction
θ polar angle
θ_s $(T_s-T_m)/(T_{s,o}-T_m)$
λ latent heat [J kg^{-1}]
ξ coordinate direction
ρ density [kg m^{-3}]
σ surface tension [N m^{-1}]
$\hat{\sigma}$ Stefan–Boltzmann constant [W m^{-2} K^{-4}]
σ_m surface tension at melting temperature [N m^{-1}]
τ dimensionless time.

Subscripts
a ambient
b ball
i liquid–solid interface
L liquidus
m melting condition
o initial; $\theta = 0$
s solid; outer surface
S solidus
v void
w wire.

Superscript
* dimensionless quantity.

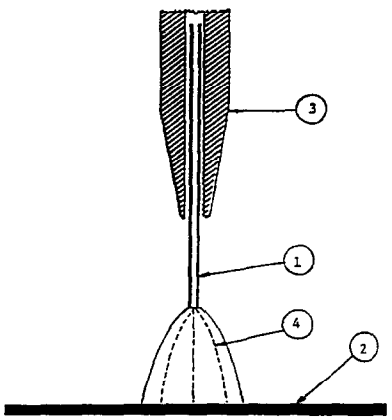

1. wire electrode
2. wand electrode
3. ceramic capillary
4. electric discharge

Fig. 1. Schematic representation of this problem.

The melting and solidification sequences are obtained from high speed cinematography. Computer controlled data acquisition and measurement are used. The temperature measurements in the wire using type K thermocouples enable us to determine the heat flux from the electrical discharge to the wire and the convective heat loss from the side of the wire to the ambient.

An important contribution of this study is thought to lie in the demonstration of suitable analytical and numerical procedures for tracking mobile interfaces involving melting and solidification. Also, an important practical application of this modeling arises in semiconductor chip assembly and packaging. In this fabrication process, the solidified ball is pressed onto the proper bond pad on the microchip to make a ball bond. (A second bond is then made onto a lead frame to connect the chip circuit to the outside world.) To properly design automatic wire bonding machines with a high throughput, parameters must be established to assure perfect balls every time. A detailed understanding of the various heat transfer processes and mechanisms involved will enable the development of optimal design conditions and considerable savings are possible (see Jog *et al.* [1]).

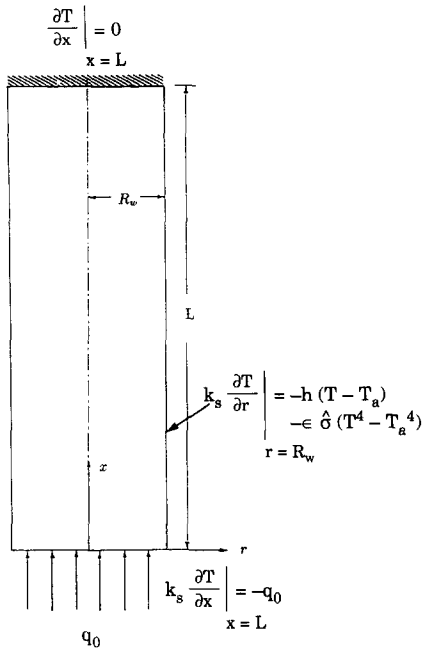

Fig. 2. Schematic of the transient heating of the wire.

2. ANALYTICAL/NUMERICAL STUDIES

2.1. *Initial heat-up and melting of the wire*

First, we are concerned with the temperature response of a cylinder, subject to heat input at one end and heat loss from its side by radiation and natural convection. Consider a homogeneous solid circular cylinder, initially at a uniform, constant temperature equal to that of the ambient (see Fig. 2). At time $t = 0$, a uniform and constant heat flux is applied to its bottom face. The cylinder loses heat from its side through natural convection and radiation. The radiative loss process is nonlinear. Since the cylinder radius is much smaller than its length, we think of it as a wire ($L/R_w \sim 100$), where L is the length of the wire and R_w is the radius. Conduction is due mainly to the temperature gradient along its axial direction. Energy conservation in the wire is expressed by

$$\frac{\partial T}{\partial \tau} = \frac{\partial^2 T}{\partial x^2} - \frac{2R_w}{k_s}\{hT + \varepsilon\hat{\sigma}[(T+T_a)^4 - T_a^4]\} \quad (1)$$

where length x and time τ are dimensionless. Equation (1) is subject to the initial condition

$$T = T_a - T_m \quad \text{at} \quad \tau = 0 \quad (2)$$

the boundary condition at its bottom face before melting

$$\left.\frac{\partial T}{\partial x}\right|_{x=0} = -\frac{q_0 R_w}{k_s} \quad (3)$$

or during the melting process

$$T|_{x=x_i(\tau)} = 0 \quad (4)$$

and the boundary condition at the other end of the wire

$$\left.\frac{\partial T}{\partial x}\right|_{x=L} = 0 \quad (5)$$

together with the interface condition

$$\frac{\partial x}{\partial \tau} = \frac{k_s}{\alpha_s \rho_s \lambda}\left.\frac{\partial T}{\partial x}\right|_{x=x_i(\tau)} + \frac{qR_w}{\alpha_s \rho_s \lambda}. \quad (6)$$

Here $x_i(\tau)$ denotes the instantaneous location of the solid–liquid interface, T_m is the melting temperature of the wire, T_a is the ambient temperature, λ is the latent heat for melting and ρ_s is the density of the solid. In equations (1)–(6), T, x and τ are defined as $T^* = (T - T_m)$, $x^* = (x/R_w)$, $\tau = (t\alpha_s/R_w^2)$, where R_w is the radius of the wire, α_s is the thermal diffusivity of the solid and the asterisks have been suppressed. Also, k_s is the thermal conductivity of the solid, h is the heat transfer coefficient for convective heat loss from the wire surface (see Ramakrishna *et al.* [2]), ε is the emissivity of the wire material, $\hat{\sigma}$ is the Stefan–Boltzmann constant, q_0 is the heat flux from the arc to the wire during the heat-up process and q is the heat flux from the melt to the wire during the melting and solidification processes. Estimation of q_0 itself is discussed in papers by Huang *et al.* [3], Jog *et al.* [4, 5] and Ramakrishna *et al.* [6, 7].

During melting, the interface location ($x = x_i(\tau)$) moves in the positive x-direction with time (in a fixed coordinate frame). The moving interface $x = x_i(\tau)$ is immobilized by using the following transformation:

$$\hat{x} = \frac{x - x_i(\tau)}{L - x_i(\tau)}, \quad (0 \leqslant \hat{x} \leqslant 1) \quad (7)$$

where x, $x_i(\tau)$ and L refer to a fixed coordinate system. In the transformed coordinates, equation (1) becomes

$$\frac{\partial T}{\partial \tau} = \frac{1}{(L-x_i)^2}\frac{\partial^2 T}{\partial \hat{x}^2} + \frac{dx_i}{d\tau}\frac{1-\hat{x}}{L-x_i}\frac{\partial T}{\partial \hat{x}} - \frac{2R_w}{k_s}\{hT + \varepsilon\hat{\sigma}[(T+T_a)^4 - T_a^4]\}. \quad (8)$$

Equations (3)–(6) become

$$\left.\frac{\partial T}{\partial \hat{x}}\right|_{\hat{x}=0} = -\frac{qR_w L}{k_s} \quad (9)$$

$$T|_{\hat{x}=0} = 0 \quad (10)$$

$$\left.\frac{\partial T}{\partial \hat{x}}\right|_{\hat{x}=1} = 0 \quad (11)$$

and

$$\frac{\partial x_i}{\partial \tau} = \frac{k_s}{\alpha_s \rho_s \lambda (L - x_i)}\left.\frac{\partial T}{\partial \hat{x}}\right|_{\hat{x}=0} + \frac{qR_w}{\alpha_s \rho_s \lambda}. \quad (12)$$

Equations (8)–(12) are solved by the Crank–Nicolson technique. This enables us to determine the temperature–time history in the solid, the instantaneous location of the interface, and thus the instantaneous volume of the melt, V_l, i.e.

$$V_l(\tau) = \pi R_w^3 x_i(\tau)\left(\frac{\rho_s}{\rho_l}\right) \tag{13}$$

where subscripts s and l refer to the solid and liquid phases, respectively.

3. SHAPE OF THE MELT

The equilibrium form of the surface of the molten metal and hence the instantaneous shape of the melt, may be determined by solving the variational problem of minimizing the total energy (Weinstock [8]). The energy of an incompressible molten metal sphere depends only on the volume of the fluid, and not on the shape of its surface. This energy consists of: (a) the surface free energy $= \int \sigma \, ds$, where s is the surface area and σ is the surface tension coefficient and (b) the external field energy $= g\rho_l \int x \, dV_l$, where ρ_l is the density of the liquid, g is the acceleration due to gravity and V_l is the instantaneous volume of the molten liquid. Thus the equilibrium condition may be written as

$$\Phi = \int \sigma \, ds + g\rho_l \int x \, dV_l = \text{minimum}. \tag{14}$$

The minimum is to be determined subject to the constraint condition that, at any given instant,

$$V_l = \int dV_l = \text{constant}. \tag{15}$$

We now assume that the liquid–solid interface remains flat, and the surface is given by (see Fig. 3)

$$r = r(x). \tag{16}$$

Assuming axial symmetry, the infinitesimal surface area ds is given by

$$ds = 2\pi r(x)\sqrt{1+\left(\frac{\partial r}{\partial x}\right)^2}\, dx \tag{17}$$

and the infinitesimal volume dV_l is

$$dV_l = \pi r(x)^2 \, dx. \tag{18}$$

Let $r^* = r/R_w$, $x^* = x/R_w$ and D^* be the point of intersection of $r^* = r^*(x^*)$ with $r^* = 0$ on the negative x axis, and we omit the asterisks for convenience in the following discussion. Let the parameter which represents the variation of the surface tension be defined as

$$\varepsilon = \frac{\sigma - \sigma_m}{\sigma_m} \tag{19}$$

where σ is the surface tension at the local temperature and σ_m is the surface tension at the melting temperature. With the above, equation (14) for energy may be written as

$$\Pi = \frac{\Phi}{\pi R_w^2 \sigma_m} = \int_0^D 2r(x)\sqrt{1+\left(\frac{\partial r}{\partial x}\right)^2}\, dx + \int_0^D 2\varepsilon r(x)\sqrt{1+\left(\frac{\partial r}{\partial x}\right)^2}\, dx - \int_0^D Eo\, x r^2 \, dx. \tag{20}$$

The Eötvös number Eo, which represents the ratio of gravity effect to the surface tension, is defined as

$$Eo = \frac{g\rho_l R_w^2}{\sigma_m}. \tag{21}$$

The constraint condition (16) becomes

$$V = \frac{V_l}{\pi R_w^3} = \int_0^D r^2 \, dx. \tag{22}$$

Minimizing the energy Π in equation (20) subject to the constraint condition, equation (22), gives the Euler–Lagrange equation for $r(x)$:

$$r\frac{d^2r}{dx^2} - \left(\frac{dr}{dx}\right)^2 - 1 - \Gamma r\left[1+\left(\frac{dr}{dx}\right)^2\right]^{3/2} + \varepsilon\left[r\frac{d^2r}{dx^2} - \left(\frac{dr}{dx}\right)^2 - 1\right] + \frac{d\varepsilon}{dx} r\left[\frac{dr}{dx} + \left(\frac{dr}{dx}\right)^3\right] + Eo\, x r\left[1+\left(\frac{dr}{dx}\right)^2\right]^{3/2} = 0. \tag{23}$$

Equation (23) is subject to the constraint condition equation (15) and the conditions

$$r(0) = 1 \tag{24}$$

$$r(D) = 0 \tag{25}$$

and

$$1 \Big/ \left|\frac{dr}{dx}\right|_{x=D} = 0 \tag{26}$$

where Γ is the undetermined Lagrange multiplier.

The instantaneous shape of the molten metal is determined by noting that the molten liquid has very high surface tension and this surface tension decreases only slightly with increasing temperature. Typically for metallic wires, for example aluminum, Eo is in the range 10^{-5}–10^{-1} for a drop of radius R from 10^{-5} to 10^{-3} m, respectively. For aluminum, the variation of surface tension with temperature can be expressed as (Hatch [9])

$$\sigma = [868 - 0.152(T_s - T_m)] \times 10^{-3} \text{ N m}^{-1} \tag{27}$$

where T_s is the local surface temperature and T_m is the melting temperature in K. For $\Delta T = T_s - T_m \approx 10^2$ K, $\varepsilon \approx 10^{-2}$ for aluminum. At such small Eo and ε, the departure from sphericity associated with the roll up of the melt and subsequent ball formation may be

regarded as a small perturbation. We now discuss a perturbation scheme to reflect this feature. Let $T_{s,o}$ be the surface temperature on the x-axis and $\theta_s = (T_s - T_m)/(T_{s,o} - T_m)$. Then δ is defined by

$$\varepsilon = \delta\theta_s. \tag{28}$$

Since surface tension σ is linear in T_s, for a given $(T_{s,o} - T_m)$, δ is fixed in value, and the following relation is applicable:

$$\frac{d\varepsilon}{dx} = \delta\frac{\partial\theta_s}{\partial x}. \tag{29}$$

Substituting equations (28) and (29) into equation (23), the Euler–Lagrange equation may be rewritten as

$$r\frac{d^2r}{dx^2} - \left(\frac{dr}{dx}\right)^2 - 1 - \Gamma r\left[1+\left(\frac{dr}{dx}\right)^2\right]^{3/2} + \delta\left\{\theta_s\left[r\frac{d^2r}{dx^2} - \left(\frac{dr}{dx}\right)^2 - 1\right] + \frac{d\theta_s}{dx}r\left[\frac{dr}{dx} + \left(\frac{dr}{dx}\right)^3\right]\right\} + Eo\,xr\left[1+\left(\frac{dr}{dx}\right)^2\right]^{3/2} = 0. \tag{30}$$

This equation and the appropriate boundary conditions are expanded in terms of the small parameters δ and Eo, and are solved up to first order. We write the perturbation expansion

$$r = r_{00} + r_{10}\delta + r_{10}Eo + \ldots \tag{31}$$

where r_{00} is the zeroth-order solution, and the finite quantities r_{01} and r_{10} represent the change due to surface tension δ and gravity Eo, respectively. Substituting equation (31) and its derivatives into equation (30), the governing equation and boundary conditions may be rewritten as follows.

3.1. *Zeroth-order solution*

The equation for the zeroth-order solution is

$$r_{00}\frac{d^2r_{00}}{dx^2} - \left(\frac{dr_{00}}{dx}\right)^2 - 1 - \Gamma r_{00}\left[1+\left(\frac{dr_{00}}{dx}\right)^2\right]^{3/2} = 0 \tag{32}$$

and the corresponding boundary conditions are

$$r_{00}(0) = 1 \tag{33}$$

$$r_{00}(D) = 0 \tag{34}$$

and

$$1\Big/\left.\frac{dr_{00}}{dx}\right|_{x=D} = 0. \tag{35}$$

An analytical solution can be found based on the fact that the independent variable does not appear in the nonlinear ordinary differential equation (32). The analytical solution of this problem yields

$$r_{00}^2(x) + (x \pm \sqrt{R_0^2 - 1})^2 = R_0^2 \tag{36}$$

where R_0 is determined by side conditions. For $V < \frac{2}{3}$, we have to choose the negative sign before the radical in equation (36). The solution for R_0 is then given by

$$\tfrac{1}{3}H^2(3R_0 - H) = V. \tag{37}$$

For $V > \frac{2}{3}$, we have to choose the positive sign before the radical in equation (36). The solution for R_0 is now given by

$$\tfrac{4}{3}R_0^3 - \tfrac{1}{3}H^2(3R_0 - H) = V. \tag{38}$$

In equations (37) and (38)

$$H = R_0 - \sqrt{R_0^2 - 1}. \tag{39}$$

3.2. *First-order solution with surface tension effect* (δ)

The governing equation for r_{10} is

$$\frac{d^2r_{10}}{dx^2} - \left[\frac{4(x \pm \sqrt{R_0^2-1})}{R_0^2 - (x \pm \sqrt{R_0^2-1})^2}\right]\frac{dr_{10}}{dx} + \left[\frac{R_0^2}{(R_0^2 - (x \pm \sqrt{R_0^2-1})^2)^2}\right]r_{10} = \frac{R_0^2}{(R_0^2 - (x \pm \sqrt{R_0^2-1})^2)^{3/2}} \times \left[(x \pm \sqrt{R_0^2-1})\frac{d\theta_s}{dx} + 2\theta_s\right]. \tag{40}$$

The boundary conditions for equation (40) are

$$r_{10} = 0 \tag{41}$$

$$\int_0^D [r_{00} + \varepsilon r_{10}]^2\,dx = V. \tag{42}$$

Equation (40) with boundary conditions (41) and (42) may be solved iteratively by using the fourth-order Runge–Kutta method.

3.3. *First-order solution with gravity effect* (Eo)

In a similar manner, the governing equation for r_{01} is

$$\frac{d^2r_{01}}{dx^2} - \left[\frac{4(x \pm \sqrt{R_0^2-1})}{R_0^2 - (x \pm \sqrt{R_0^2-1})^2}\right]\frac{dr_{01}}{dx} + \left[\frac{R_0^2}{(R_0^2 - (x \pm \sqrt{R_0^2-1})^2)^2}\right]r_{01} = \frac{R_0^3 x}{(R_0^2 - (x \pm \sqrt{R_0^2-1})^2)^{3/2}} \tag{43}$$

with the boundary conditions

$$r_{01} = 0 \tag{44}$$

$$\int_0^D [r_{00} + Eo\,r_{01}]^2\,dx = V. \tag{45}$$

and, as in the previous section, equation (43) with boundary conditions (44) and (45) may be solved iteratively by using the fourth-order Runge–Kutta

method. In this manner we determine the contour r_x for a given $V(\tau)$ at any time τ.

4. TEMPERATURE IN THE MELT

In this section, we are concerned with the temperature response of the growing molten ball. The melt, whose instantaneous shape is determined in the previous section by the minimum energy method, is subject to heat input at its outer surface from the electrical discharge and heat loss by conduction up the wire. The heat flux q used in equation (6) and the θ_s in equation (28) are derived from the results of this section.

With reference to Fig. 3, the energy equation for the melt is

$$\frac{\partial T_l}{\partial \tau} = \alpha_{ls}\left(\frac{\partial^2 T_l}{\partial r^2} + \frac{1}{r}\frac{\partial T_l}{\partial r} + \frac{\partial^2 T_l}{\partial x^2}\right) \tag{46}$$

subject to

$$T_l = 0 \quad \text{at} \quad \tau = 0 \tag{47}$$

$$\frac{\partial T_l}{\partial n_b} = \frac{q_b R_w}{k_l} \tag{48}$$

and, at the solid–liquid interface,

$$T_l = 0 \quad \text{at} \quad x = 0. \tag{49}$$

The heat flux from the melt conducted into the wire, which is used in an earlier section for heat input, is

$$q = \frac{k_l}{R_w}\frac{\partial T_l}{\partial n_w} \tag{50}$$

where subscript l represents the liquid phase, $\alpha_{ls} = \alpha_l/\alpha$, and n_b and n_w denote the outward drawn normals to the surface $r = r(x)$. In equation (48), q_b is the heat flux received by the surface of the melt and it varies with time. For arc heating, the value of q_b may be assumed to be related to q_{max} (the heat flux at the bottom point D) by

$$q_b = q_{max}\cos\frac{\theta}{2}. \tag{51}$$

Now q_{max} is related to the applied heat flux value q at $\tau = 0$ by

$$q_{max} = \frac{3q_0}{8R_0^2\{1-\cos^3[(\pi-\theta_i)/2]\}} \tag{52}$$

where

$$\theta_i = \arcsin\frac{R_w}{R_0} \tag{53}$$

signifies the direction of the vector locating the boundary between the melt and the solid.

Equation (46), subject to equations (48)–(53), is solved by the ADI method using a body-fitted coordinate system. The numerical mapping technique employed is based on a method of automatic numerical generation of a general curvilinear coordinate system and first developed and applied to fluid mechanical problems by Thompson *et al.* [10]. The body-fitted coordinate system is created by numerically solving the following system of two elliptic equations:

$$a_{11}x_{\xi\xi} - 2a_{12}x_{\xi\eta} + a_{22}x_{\eta\eta} + J^2(Px_\xi + Qx_\eta) = 0 \tag{54}$$

$$a_{11}r_{\xi\xi} - 2a_{12}r_{\xi\eta} + a_{22}r_{\eta\eta} + J^2(Pr_\xi + Qr_\eta) = 0. \tag{55}$$

The coefficients are defined as

$$\begin{aligned} a_{11} &= x_\eta^2 + r_\eta^2 \\ a_{12} &= x_\xi x_\eta + r_\xi r_\eta \\ a_{22} &= x_\xi^2 + r_\xi^2 \\ J &= x_\xi r_\eta - r_\xi x_\eta. \end{aligned} \tag{56}$$

The functions P and Q are coordinate control functions which may be chosen so as to cause the coordinate lines to concentrate in certain parts of the domain where rapid variations of a given property are expected. The transformed equations in the rectangular, uniformly spaced computational domain (ξ, η) are

$$\begin{aligned} \frac{\partial T_l}{\partial \tau} = {} & \frac{\alpha_{ls}a_{11}}{J^2}\frac{\partial^2 T_l}{\partial \xi^2} - \frac{2\alpha_{ls}a_{12}}{J^2}\frac{\partial^2 T_l}{\partial \xi\,\partial \eta} + \frac{\alpha_{ls}a_{22}}{J^2}\frac{\partial^2 T_l}{\partial \eta^2} \\ & + \left[\frac{r_\eta \dot{x}}{J} + \alpha_{ls}Q - \frac{x_\eta \dot{r}}{J} + \frac{\alpha_{ls}r_\eta}{xJ}\right]\frac{\partial T_l}{\partial \xi} \\ & + \left[\frac{x_\xi \dot{r}}{J} + \alpha_{ls}P - \frac{r_\xi \dot{x}}{J} - \frac{\alpha_{ls}r_\xi}{xJ}\right]\frac{\partial T_l}{\partial \eta} \end{aligned} \tag{57}$$

subject to

$$T_l = 0 \quad \text{at} \quad \tau = 0 \tag{58}$$

$$\left[a_{22}\frac{\partial T_l}{\partial \eta} - a_{12}\frac{\partial T_l}{\partial \xi}\right]_{\eta=1} = \frac{q_b R_w}{k_l}J\sqrt{a_{22}} \tag{59}$$

$$T_l = 0 \quad \text{at} \quad \eta = 0 \tag{60}$$

$$T_l = 0 \quad \text{at} \quad \xi = 1 \tag{61}$$

and the axisymmetric condition

$$\left.\frac{\partial T_l}{\partial \xi}\right|_{\xi=0} = 0. \tag{62}$$

These equations are solved by the ADI method. After the temperature distribution in the melt is obtained, the heat flux q from the melt conducted into the wire and ΔT_s are calculated.

5. SOLIDIFICATION OF THE MELT

In the case of spherically symmetric solidification of a pure metal, when the temperature of the melt drops below the fusion temperature, the solid phase forms and grows radially inward. As this occurs, latent heat is released at the liquid–solid interface. The phase change interface moves with a velocity determined by the energy balance there. During solidification, there

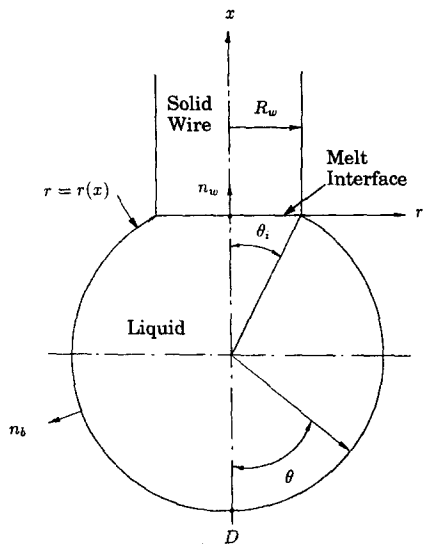

Fig. 3. Schematic of the ball during formation with coordinates.

is an increase in density and a void may form in the melt. The instantaneous void center will coincide with the centroid of the molten mass. A purely radial flow analysis with spherically shaped melts has been discussed by Heurtault *et al.* [11] and Huang *et al.* [12]. But, in view of the non-uniform heat loss from the melt surface, a one-dimensional formulation is inadequate. We now provide a more detailed analysis.

The governing equation for the liquid phase and the solid phase are governed by

$$\frac{\partial T_l}{\partial \tau} = \alpha_{ls}\left(\frac{\partial^2 T_l}{\partial r^2} + \frac{1}{r}\frac{\partial T_l}{\partial r} + \frac{\partial^2 T_l}{\partial x^2}\right) \tag{63}$$

and

$$\frac{\partial T_s}{\partial \tau} = \frac{\partial^2 T_s}{\partial r^2} + \frac{1}{r}\frac{\partial T_s}{\partial r} + \frac{\partial^2 T_s}{\partial x^2} \tag{64}$$

respectively. Equations (63) and (64) are subject to the following boundary conditions. At the liquid–ambient and solid–ambient interfaces

$$\left.\frac{\partial T_j}{\partial n_b}\right|_{\text{ball surface}} = -\frac{R_w}{k_j}\{hT_j + \varepsilon\sigma[(T_j + T_a)^4 - T_a^4]\},$$

$$j = l \text{ or } s \tag{65}$$

where n_b is the outward normal to the ball (see Fig. 3). At the wire–melt junction

$$T_s|_{\text{ball}} = T|_{\text{wire}}. \tag{66}$$

The heat flux from the melt conducted into the wire, which is used in solving the wire temperature for heat input, is

$$q = -\frac{k_s}{R_w}\frac{\partial T_s}{\partial n_w}. \tag{67}$$

At the solid–liquid interface

$$T_l = T_s = 0 \tag{68}$$

and

$$k_s\frac{\partial T_s}{\partial n_w} - k_l\frac{\partial T_l}{\partial n_w} = \rho_s \lambda v_{nw} \tag{69}$$

where $\partial/\partial n_w$ denotes the normal derivative at the interface and n_w denotes the normal to the interface. Here, λ and v_{nw} are latent heat and normal component of the velocity of the interface motion, and subscripts s and l denote the solid and liquid phases, respectively.

The body-fitted coordinate system is used here. For convenience, the analysis can be divided into three regions of study, namely the liquid, the liquid–solid interface and the solid.

5.1. *Solid and liquid regions*

The transformed governing equations in the rectangular, uniformly spaced computational domain (ξ, η) are

$$\frac{\partial T_j}{\partial \tau} = \frac{\alpha_{ls}a_{11}}{J^2}\frac{\partial^2 T_j}{\partial \xi^2} - \frac{2\alpha_{ls}a_{12}}{J^2}\frac{\partial^2 T_j}{\partial \xi\,\partial \eta} + \frac{\alpha_{ls}a_{22}}{J^2}\frac{\partial^2 T_j}{\partial \eta^2} + \left[\frac{r_\eta \dot{x}}{J} + \alpha_{ls}Q - \frac{x_\eta \dot{r}}{J} + \frac{\alpha_{ls}r_\eta}{xJ}\right]\frac{\partial T_j}{\partial \xi} + \left[\frac{x_\xi \dot{r}}{J} + \alpha_{ls}P - \frac{r_\xi \dot{x}}{J} - \frac{\alpha_{ls}r_\xi}{xJ}\right]\frac{\partial T_j}{\partial \eta} \quad j = l \text{ or } s \tag{70}$$

subject to

$$\left[a_{22}\frac{\partial T_l}{\partial \eta} - a_{12}\frac{\partial T_l}{\partial \xi}\right]_{\eta = 1} = \frac{q_b R_w}{k_l} J\sqrt{a_{22}} \tag{71}$$

$$T_j = T|_{\text{wire}} \quad \text{at} \quad \eta = 0 \quad j = l \text{ or } s \tag{72}$$

$$T_j = T|_{\text{wire}} \quad \text{at} \quad \xi = 1 \quad j = l \text{ or } s \tag{73}$$

and the axisymmetric condition

$$\left.\frac{\partial T_j}{\partial \xi}\right|_{\xi = 0} = 0 \quad j = l \text{ or } s. \tag{74}$$

The governing equation with boundary conditions are solved by the ADI method. Marangoni convection in the liquid has been neglected since it is unimportant for the problem under consideration.

5.2. *Region near the solid–liquid interface*

The interface condition appropriate for a general nonorthogonal curvilinear coordinate system has been developed in Huang *et al.* [13]. If the interface is defined as $F(\xi, \eta, \tau) = \xi - \Gamma(\eta, \tau) = 0$, equations (68) and (69) in the (ξ, η) coordinate system become

$$\left[a_{11} + a_{22}\left(\frac{\partial \Gamma}{\partial \eta}\right)^2 + 2a_{12}\frac{\partial \Gamma}{\partial \eta}\right] \cdot \left[k_s\frac{\partial T_s}{\partial \xi} - k_l\frac{\partial T_l}{\partial \xi}\right] = \alpha_s\rho_s\lambda J^2\frac{\partial \Gamma}{\partial \tau}. \tag{75}$$

If $F(\xi, \eta, \tau) = \eta - \Lambda(\xi, \tau) = 0$, equations (70) and (71) in the (ξ, η) coordinate system can be rewritten as

$$\left[a_{11}\left(\frac{\partial\Lambda}{\partial\xi}\right)^2+a_{22}+2a_{12}\frac{\partial\Lambda}{\partial\xi}\right]\cdot\left[k_s\frac{\partial T_s}{\partial\eta}-k_l\frac{\partial T_l}{\partial\eta}\right]=\alpha_s\rho_s\lambda J^2\frac{\partial\Lambda}{\partial\tau}. \quad (76)$$

The method that continuously tracks the moving interface has been used and this generally yields accurate results. This method leads to a set of nonlinear algebraic equations involving the unknown nodal temperatures and the interface location. The equations applicable at the interface are isolated by making an energy balance at the interface and the surrounding nodal locations. The method accurately tracks the interface along both of the coordinate axes thereby eliminating the need for interpolating its location between coordinate axes. The energy equation is used implicitly in alternating directions similar to the conventional ADI method. This avoids the need for iterations at ordinary nodes away from the interface.

At any time τ let the interface be near the nodal location (p, q) and let its distance measured along ξ and η coordinates be $\beta_{p,q}\Delta\xi$ and $\gamma_{p,q}\Delta\eta$ such that $-0.5<\beta_{p,q}<0.5$ and $-0.5<\gamma_{p,q}<0.5$. For simplicity, the subscripts on β and γ are dropped in the text that follows. The first and second order derivatives of the temperature near the solid–liquid interface can be obtained by using a Taylor series expansion. Here, we assume that node $(p-1,q)$ or $(p,q-1)$ is in the liquid phase, and $(p+1,q)$ or $(p,q+1)$ is in the solid phase.

Liquid phase near the interface for ξ-direction

$$\left.\frac{\partial T_l}{\partial\xi}\right|_{\text{interface}}=\frac{1}{\Delta\xi}\left[\frac{1+\beta}{2+\beta}T_{p-2,q}-\frac{2+\beta}{1+\beta}T_{p-1,q}\right] \quad (77)$$

$$\left.\frac{\partial^2 T_l}{\partial\xi^2}\right|_{\text{interface}}=\frac{2}{\Delta\xi^2}\left[\frac{1}{2+\beta}T_{p-2,q}-\frac{1}{1+\beta}T_{p-1,q}\right]. \quad (78)$$

Solid phase near the interface for ξ-direction

$$\left.\frac{\partial T_s}{\partial\xi}\right|_{\text{interface}}=\frac{1}{\Delta\xi}\left[\frac{2-\beta}{1-\beta}T_{p+1,q}-\frac{1-\beta}{2-\beta}T_{p+2,q}\right] \quad (79)$$

$$\left.\frac{\partial^2 T_s}{\partial\xi^2}\right|_{\text{interface}}=\frac{2}{\Delta\xi^2}\left[\frac{1}{2-\beta}T_{p+2,q}-\frac{1}{1-\beta}T_{p+1,q}\right]. \quad (80)$$

Similarly, liquid phase near the interface for η-direction

$$\left.\frac{\partial T_l}{\partial\eta}\right|_{\text{interface}}=\frac{1}{\Delta\eta}\left[\frac{1+\gamma}{2+\gamma}T_{p,q-2}-\frac{2+\gamma}{1+\gamma}T_{p,q-1}\right] \quad (81)$$

$$\left.\frac{\partial^2 T_l}{\partial\eta^2}\right|_{\text{interface}}=\frac{2}{\Delta\eta^2}\left[\frac{1}{2+\gamma}T_{p,q-2}-\frac{1}{1+\gamma}T_{p,q-1}\right]. \quad (82)$$

Solid phase near the interface for η-direction

$$\left.\frac{\partial T_s}{\partial\eta}\right|_{\text{interface}}=\frac{1}{\Delta\eta}\left[\frac{2-\gamma}{1-\gamma}T_{p,q+1}-\frac{1-\gamma}{2-\gamma}T_{p,q+2}\right] \quad (83)$$

$$\left.\frac{\partial^2 T_s}{\partial\eta^2}\right|_{\text{interface}}=\frac{2}{\Delta\eta^2}\left[\frac{1}{2-\gamma}T_{p,q+2}-\frac{1}{1-\gamma}T_{p,q+1}\right]. \quad (84)$$

For tracking the interface movement along the two coordinate axes, the interface conditions (75) and (76), and the energy equations (70), written in alternate directions, are solved by the Crank–Nicolson method. In the ξ-direction, three unknowns, β, $T_{p-1,q}$ and $T_{p+1,q}$, are solved by the following three equations: interface energy equation (75), liquid-phase energy equation and solid-phase energy equation (70). Using equations (77)–(80), these three equations [(70), (75) and (76)] are transformed into finite difference formulae for numerical calculation. Similarly, in the η-direction, equations (70) for liquid and solid phases and (76) are used for solving for three unknowns, γ, $T_{p,q-1}$ and $T_{p,q+1}$, and equations (81)–(84) are used to transform them into finite difference formulae.

6. SOLIDIFICATION IN A BINARY ALLOY SYSTEM

Our solidification analysis may be extended to cover binary alloy systems. Unlike pure metals which solidify at a discrete temperature, alloys solidify over a range bounded by the liquidus and solidus temperatures. The cooling of the liquid metal alloy is described by equations similar to the above set. We have to replace the thermophysical properties of the pure metal with those of the alloy. During the initial phase of alloy solidification, only the liquid and mushy regions exist. Here the mushy region is understood to represent a homogeneous mixture of the liquid and the solid in coexistence in relative proportions determined by a linear interpolation between the liquidus and solidus temperatures. The mushy region replaces the sharply defined liquid–solid interface existing in the case of a pure metal. The thermophysical properties in the mushy regions are defined as

$$c_p=(1-f_l)c_{p,s}+f_l c_{p,l}+\frac{h_{LS}}{\Delta T_{LS}} \quad (85)$$

$$k=(1-f_l)k_s+f_l k_l \quad (86)$$

and

$$\rho=(1-f_l)\rho_s+f_l\rho_l \quad (87)$$

where $h_{LS}=h_L-h_S$, $\Delta T_{LS}=T_L-T_S$ and T_L and T_S are the liquidus and solidus temperatures, respectively and f_l is the fraction of the liquid in the mush. We may determine f_l by using the lever rule (linear interpolation) between T_L and T_S. It is assumed that the latent heat release is independent of temperature in the range T_L to T_S. The remaining thermophysical properties are obtained by interpolating between their values for the solid and liquid phases, depending upon

the local liquid fraction, f_l. With the thermophysical properties established, we may use the transient heat conduction equation to describe the temperature evolution in the mushy region.

7. SUMMARY AND CONCLUSIONS

Given the heat flux from the electric discharge to the bottom of the wire and the convective heat loss from the exposed side of the wire to the ambient, we have shown how to calculate the entire temperature and phase history of the metal. The calculation encompasses initial heating, melting, ball roll-up, cooling and solidification. The two inputs are obtained from matching the computed results with experimentally measured temperature time histories. The details are given in Part II. With the input data so obtained, we can compare computed and observed ball shape profiles as a function of time. This comparison is displayed in Part II where we have presented our conclusions of this entire study.

REFERENCES

1. M. A. Jog, I. M. Cohen and P. S. Ayyaswamy, Heat transfer in wire bonding process, *ASME J. Electron. Packaging* **116,** 44–48 (1994).
2. K. Ramakrishna, I. M. Cohen and P. S. Ayyaswamy, Temperature response of a heated cylinder subject to side cooling: asymptotic and numerical solutions, *ASME J. Heat Transfer* **111,** 592–597 (1989).
3. L. J. Huang, M. A. Jog, I. M. Cohen and P. S. Ayyaswamy, Effect of polarity on heat transfer in the ball formation process, *ASME J. Electron. Packaging* **113,** 33–39 (1991).
4. M. A. Jog, I. M. Cohen and P. S. Ayyaswamy, Breakdown of a wire-to-plane discharge: transient effects, *Phys. Fluids B* **3,** 3532–3536 (1991).
5. M. A. Jog, I. M. Cohen and P. S. Ayyaswamy, Electrode heating in a wire-to-plane arc, *Phys. Fluids B* **4,** 465–472 (1992).
6. K. Ramakrishna, I. M. Cohen and P. S. Ayyaswamy, Numerical methods for two-dimensional analysis of electrical breakdown in a non-uniform gap, *J. Comp. Phys.* **104,** 173–184 (1993).
7. K. Ramakrishna, I. M. Cohen and P. S. Ayyaswamy, Effect of negative ions on electrical breakdown in a non-uniform air gap between a wire and a plane, *Phys. Plasmas* **1,** 1349–1358 (1994).
8. R. Weinstock, *Calculus of Variations.* McGraw-Hill, New York (1952).
9. *Aluminum—Properties and Physical Metallurgy* (Edited by J. E. Hatch). American Society for Metals, Metals Park, OH (1984).
10. J. F. Thompson, F. C. Thames and C. W. Mastin, Automatic numerical generation of body-fitted curvilinear coordinate system for fields containing any number of arbitrary two-dimensional bodies, *J. Comp. Phys.* **15,** 299–319 (1974).
11. S. Heurtault, J. M. Badie, A. Rouanet and G. Arnad, Solidification de sphères liquides surchauffées à caracteristiques physiques variables, *Int. J. Heat Mass Transfer* **25,** 1671–1676 (1982).
12. L. J. Huang, K. Ramakrishna, P. S. Ayyaswamy and I. M. Cohen, An analysis of solidification of metals and alloys accompanied by density change and void formation, *ASME J. Electron. Packaging* **111,** 119–206 (1989).
13. L. J. Huang, P. S. Ayyaswamy and I. M. Cohen, A note on the interface condition in phase change problems, *ASME J. Heat Transfer* **113,** 244–247 (1991).